

## Simulation of Mastic Erosion from Open-Graded Asphalt Mixes Using a Hybrid Lagrangian-Eulerian Finite Element Approach

N.Kringos<sup>1</sup>, A.Scarpas<sup>1</sup> and A.P.S. Selvadurai<sup>2</sup>

**Abstract:** This paper presents a numerical approach for the modeling of water flow induced mastic erosion from a permeable asphalt mix and is part of an ongoing effort to model moisture-induced damage in asphalt mixes. Due to the complex composite structure of asphalt mixtures, moisture can infiltrate in various ways into the components and have an adverse effect on its mechanical performance. Depending on the gradation of the asphalt aggregates and the mixing procedure, asphalt structures with a variable permeability may result. Open-graded asphalt mixes are designed with a high interconnected air void content to serve as a drainage layer on the pavement and are therefore frequently exposed to fast water flow fields. This paper demonstrates a numerical procedure to simulate the effects of an advection-dominated transport process on the mastic concentration within an open-graded asphalt mix. A Hybrid Lagrangian-Eulerian finite element approach is implemented with a single step reverse particle tracking scheme to solve the Lagrangian concentration tensor. The procedure is validated with two analytical studies and a numerical simulation is shown for the advective transport of mastic from an asphaltic system.

**Keyword:** Moisture-induced damage, Hybrid Lagrangian-Eulerian finite elements approach, advection dominated transport, particle tracking method

### 1 Problem identification

In countries that experience excessive rainfall each year, the asphalt wearing surfaces on roads

are often constructed of open-graded asphaltic mixes. The high permeability of these wearing surfaces ensures a rapid drainage of the water away from the surface, thereby increasing road safety, Figure 1. This water infiltration, however, has a negative effect on the material characteristics of the individual components of the asphaltic mix, damages the bonds between the components and leads to premature separation of the aggregates from the wearing surfaces, named raveling or stripping, Figure 2. To prevent this damage from occurring, insight into the different phenomena that cause raveling is needed to design more sustainable asphalt mixes and develop improved road maintenance strategies.



Figure 1: Drainage with an open graded asphalt wearing surface versus a densely graded asphalt surface [Jong 1999]

For this reason an extensive, experimental and analytical investigation on water damage in open-graded asphaltic mixes is being undertaken at Delft University of Technology in The Netherlands. The main focus of this project is the development of a Finite Element tool (acronym-RoAM; Raveling of Asphalt Mixes) as a subsystem of the finite element system developed at TU Delft, CAPA-3D [Scarpas 2000]. RoAM en-

<sup>1</sup> Faculty of Civil Engineering and Geosciences, Delft University of Technology, The Netherlands

<sup>2</sup> Department of Civil Engineering and Applied Mechanics, McGill University, Canada



Figure 2: Raveling of the asphaltic wearing surface

ables the simulation of damage due to water flow through asphaltic mixes. The raveling failure of asphaltic wearing surfaces is a complex process that involves the washing away of mastic particles from the mix, the diffusion of water through the mastic films towards the mastic-aggregate interfaces, the deterioration of both the material and the chemical characteristics of the individual components of the mix, as well a deterioration of their (physio-chemical) bonds. Furthermore, the interaction between the mechanical loads and the water pressures in the voids of the mix needs to be addressed properly.

Realizing that an asphaltic mix is frequently exposed to a water flow through the mix, it is important to identify the moisture damage inducing mechanisms that may occur in the mix. In a previous study [Kringos and Scarpas, 2005 (a), (b)] a scouring action of the mastic due to high water pressure fields was identified as one of the dominant mechanisms which contribute to the overall moisture induced damage. This paper focuses on the simulation of the erosion of the mastic and gives a detailed explanation about the numerical model that has been implemented in RoAM to simulate this loss of mastic concentration due to a water flow through the asphalt mix.

## 2 Mastic transport equation

Considering an asphaltic mix that has been exposed to a water flow field, the asphalt mastic (i.e. the mix of bitumen and fine aggregate fillers) particles may be present in an adsorbed or desorbed state. Adsorbed mastic particles are still part of the mix and contribute to the overall mix characteristics. Desorbed mastic particles have been separated from the mix and are, via the water, being transported out of the mix. They are therefore no longer contributing to the mechanical or physical material characteristics of the asphalt.

In the following, the mastic that is desorbed from the mix, and is no longer contributing to the mechanical strength of the mastic, is defined as the dissolved mastic concentration  $C_d$  and is expressed as mass of desorbed mastic  $M_d$  over a unit volume:

$$C_d = \frac{M_d}{V_w} \quad (1)$$

The mastic which is still part of the asphalt is shown as the adsorbed mastic content  $C_a$ :

$$C_a = \frac{\rho^m}{\rho_0^m} \quad (2)$$

where  $\rho_0^m$  is the reference (undamaged) density of the mastic and  $\rho^m$  is the current density of the mastic.

Consider the spatial scalar field  $C = C(\mathbf{x}, t)$  that describes the concentration of the mastic in space and time. Assuming  $C$  to be continuously differentiable, the current amount of mastic mass  $m(t)$  in a three-dimensional region  $\Omega$  with volume  $v$  given time  $t$  may be characterized by the scalar-valued function

$$m(t) = \int_{\Omega} C(\mathbf{x}, t) dv \quad (3)$$

In general, a mastic concentration at a given location in the asphalt mix consists of both desorbed and adsorbed mastic phases; i.e.

$$C(\mathbf{x}, t) = \phi S C_d + \rho_0^m C_a \quad (4)$$

where  $\phi$  is the porosity and  $S$  is the degree of saturation at time  $t$  on location  $\mathbf{x}$ .

The change of mastic mass in the volume  $\Omega$  might take place as a result of an advective and a diffusive/dispersive flux across the boundary surface  $\partial\Omega$ .

The advective flux  $F_a$  is defined as

$$F_a = \int_{\partial\Omega} C_d \mathbf{v} \cdot \mathbf{n} ds \quad (5)$$

where  $v$  is Darcy's flow velocity.

The diffusive flux  $F_d$  is defined as

$$F_d = - \int_{\partial\Omega} \mathbf{D}_m \nabla C_d \cdot \mathbf{n} ds \quad (6)$$

where  $\mathbf{D}_m$  is the mastic diffusion/dispersion tensor and  $\mathbf{n}$  denotes the outward unit normal acting along the boundary surface  $\partial\Omega$ .

Based on the mastic concentration field and the above described fluxes, the mastic mass balance can be written as

$$\begin{aligned} \frac{D}{Dt} \int_{\Omega} (\phi S C_d + \rho_0^m C_a) dv = \\ - \int_{\Omega} \text{div} (C_d \mathbf{v} - \mathbf{D}_m \nabla C_d) dv \quad (7) \end{aligned}$$

The term on the left hand side of Eq. (7) is the total time derivative of the spatial distribution of the mastic mass. By assuming incompressibility, the total time derivative is equal to the partial time derivative

$$\begin{aligned} \frac{D}{Dt} \int_{\Omega} (\phi S C_d + \rho_0^m C_a) dv = \\ \int_{\Omega} \frac{\partial}{\partial t} (\phi S C_d + \rho_0^m C_a) dv \quad (8) \end{aligned}$$

Applying the divergence theorem to Eq. (8) and after substituting in Eq. (7) gives

$$\begin{aligned} \int_{\Omega} \frac{\partial}{\partial t} (\phi S C_d + \rho_0^m C_a) dv + \int_{\Omega} \text{div} (C_d \mathbf{v}) dv \\ - \int_{\Omega} \text{div} (\mathbf{D}_m \nabla C_d) dv = 0 \quad (9) \end{aligned}$$

From the Dubois-Reymond Lemma (Selvadurai, 2000), Eq. (9) is equivalent to

$$\frac{\partial}{\partial t} (\phi S C_d + \rho_0^m C_a) + \text{div} (C_d \mathbf{v}) - \text{div} (\mathbf{D}_m \nabla C_d) = 0 \quad (10)$$

Replacing the moisture content  $\phi S$  by  $\theta$  for simplicity, the governing equation becomes

$$\frac{\partial (\theta C_d + \rho_0^m C_a)}{\partial t} + \text{div} (C_d \mathbf{v}) - \text{div} (\mathbf{D}_m \cdot \nabla C_d) = 0 \quad (11)$$

The change of the mass accumulation term of Eq. (11) can be expanded into

$$\begin{aligned} \frac{\partial (\theta C_d + \rho_0^m C_a)}{\partial t} &= \frac{\partial (\theta C_d)}{\partial t} + \frac{\partial (\rho_0^m C_a)}{\partial t} \\ &= \theta \frac{\partial C_d}{\partial t} + C_d \frac{\partial \theta}{\partial t} + \rho_0^m \frac{\partial C_a}{\partial t} \quad (12) \end{aligned}$$

The advective flux term of Eq. (11) can be written as

$$\text{div} (C_d \mathbf{v}) = C_d \text{div} \mathbf{v} + \mathbf{v} \nabla C_d \quad (13)$$

The divergence of the velocity field on the r.h.s. of Eq. (13) is known from the balance of water mass

$$\text{div} \mathbf{v} = -\tilde{\theta} \frac{\partial h}{\partial t} \quad (14)$$

whereby again incompressibility is assumed,  $h$  is the pressure head and  $\tilde{\theta}$  is the water capacity, equal to

$$\tilde{\theta} = \phi \frac{dS}{dh} \quad (15)$$

Substituting Eq. (14) into the advective flux term Eq. (13) yields

$$\text{div} (C_d \mathbf{v}) = -C_d \tilde{\theta} \frac{\partial h}{\partial t} + \mathbf{v} \nabla C_d \quad (16)$$

Substituting Eq. (16) and Eq. (12) into Eq. (11) yields the governing equation of the mastic:

$$\begin{aligned} \theta \frac{\partial C_d}{\partial t} + \rho_0^m \frac{\partial C_a}{\partial t} + \mathbf{v} \nabla C_d - \text{div} (\mathbf{D}_m \cdot \nabla C_d) \\ = \left( \tilde{\theta} \frac{\partial h}{\partial t} - \frac{\partial \theta}{\partial t} \right) C_d \quad (17) \end{aligned}$$

The relationship between the adsorbed mastic content  $C_a$  and the desorbed concentration of mastic  $C_d$  can be described via an isotherm. The type of isotherm that is used in an analysis to define this relationship (e.g. linear, Langmuir or Freundlich type) can be based on experimental data and shows the desorption characteristics of the mastic in the presence of a water field.

For simplicity, in this paper a linear relationship will be assumed

$$C_a = K_d C_d \quad (18)$$

where  $K_d$  is the desorption coefficient.

For this linear relationship Eq. (17) becomes

$$\begin{aligned} (\theta + \rho_0^m K_d) \frac{\partial C_d}{\partial t} + \mathbf{v} \nabla C_d = \\ \operatorname{div}(\mathbf{D}_m \cdot \nabla C_d) + \left( \tilde{\theta} \frac{\partial h}{\partial t} - \frac{\partial \theta}{\partial t} \right) C_d \end{aligned} \quad (19)$$

This equation describes the transport of mastic from an Eulerian (or fixed) framework.

### 3 Numerical formulations

#### 3.1 Numerical instability

The mastic transport equation, as presented in Eq. (17) combines advective (i.e. flow-field or pressure gradient driven) and diffusive (i.e. concentration gradient driven) transport of the mastic particles. This combination of advective and diffusive terms is known to cause numerical difficulties, which generally are not encountered in the governing equation of the flow field, Eq. (14). The nature of diffusion-advection equations can be conveniently characterized by the dimensionless Péclet number

$$P_e = |\mathbf{v}|h/\alpha_m \quad (20)$$

where  $\mathbf{v}$  is the velocity vector,  $h$  is a characteristic length and  $\alpha_m$  is the molecular diffusion coefficient. For example, in the case when an inert species is spreading due to molecular diffusion and advection in a one-dimensional velocity field, the governing equation can be written as

$$\frac{\partial C}{\partial t} = \frac{\partial^2 C}{\partial x^2} - P_e \frac{\partial C}{\partial x} \quad (21)$$

where  $C$  is the concentration of species.

Clearly, when  $P_e$  is small, diffusion dominates and the equation has a parabolic character. However, when  $P_e$  is large, advection dominates and the equation has a hyperbolic character. In non-uniform flow fields, like the ones occurring through an asphalt mix, where the velocity is not constant,  $P_e$  may vary from location to location both in space and time. As a result of this variation, the diffusion-advection equation may vary in character within a given field and time, being predominantly parabolic in some regions and predominantly hyperbolic in others. Physically, this means that the path of transport of a particle can vary from location to location as well as in time. This poses a challenge on the capabilities of a numerical tool to capture the concentrations accurately. Since this problem is known for quite some time, several methods have been developed over the years to treat this problem. The most conventional numerical methods for solving this problem can be classified into three major categories: Eulerian, Lagrangian or mixed Lagrangian-Eulerian [Selvadurai and Dong 2006(a), 2006(b)].

In the Eulerian approach, the equation is discretized by a finite difference or finite element grid fixed in space, where the Eulerian form of the transport equation is solved at the nodes of the grid. Since the advective and diffusive terms in this method still need to be solved simultaneously, the numerical instabilities as described above need to be avoided. The Eulerian approach often uses weighting functions that are one or two orders higher than the base functions as a form of stabilization, where the weighting factors are dependent on the direction of the flow. A popular method within this category is the streamline upwinding by the Petrov-Galerkin method (SUPG) [Hughes 1987; Belytschko 2000].

In the Lagrangian approach, either a deforming grid or a fixed grid in deforming coordinates is used, where the physical quantities are computed at a set of point moving with the fluid. The numerical instabilities are in this case avoided because the advective term is no longer treated explicitly by solving the Lagrangian form of the transport equation in grids moving with the particles. Even

though the Lagrangian approach is more powerful than the Eulerian, it is less popular because of the complexities arising from the highly distorting grid, including mesh tangling.

In a mixed Lagrangian-Eulerian approach [Neuman, 1981], [Neuman, 1984], [Hughes, 1987], [Belytschko, 2000], a combination of the two above methods is used, whereby the benefits of both are combined without their disadvantages. The method employs, just like the Eulerian method, a fixed grid. However, the advective term is computed via a Lagrangian approach using a particle tracking method. This way the advective term vanishes from the governing equation, which then can be solved with either a finite difference or a finite element or other variant numerical method.

### 3.2 Stabilized hybrid Lagrangian-Eulerian formulation

In the research described in this paper, a Hybrid Lagrangian-Eulerian approach has been implemented, where the Lagrangian concentrations are computed via a single-step reverse tracking method [Galeati, 1992] and the diffusive part is computed via a Eulerian finite element method.

Lagrangian-Eulerian methods generally solve the advective part of the problem by a ‘method of characteristics’ and the diffusive part by Eulerian grid methods, such as finite elements. The traditional method of characteristics is explicit and tracks particles forward in a manner which is computing intensive. Therefore, in this paper a modified method is used which is implicit and known to be unconditionally stable. In this method the path lines of the particles are traced backwards according to a single step reverse algorithm [Neuman 1981], [Douglas and Russel 1982], [Baptista et al. 1984], [Casulli 1987].

Following Neuman [1981, 1984], the total time derivative of  $C_d$  is computed by

$$\begin{aligned} \frac{DC_d(\mathbf{x},t)}{Dt} &= \frac{\partial C_d(\mathbf{x},t)}{\partial t} + \frac{\partial C_d(\mathbf{x},t)}{\partial \mathbf{x}_i} \frac{\partial \mathbf{x}_i}{\partial t} \\ &= \frac{\partial C_d(\mathbf{x},t)}{\partial t} + \nabla C_d \mathbf{v}^* \end{aligned} \quad (22)$$

where  $\mathbf{v}^*$  is the velocity of a particle that moved

in the flow field, also known as the ‘seepage velocity’ and is equal to

$$\mathbf{v}^* = \frac{\mathbf{v}}{(\theta + \rho_0^m K_d)} \quad (23)$$

Eq. (22) describes changes with time along particle lines. For convenience, the arguments  $(\mathbf{x}, t)$  of the tensor quantities are suppressed in the following.

The partial derivative  $\frac{\partial C_d}{\partial t}$  can therefore, according to the above, also be written as

$$\frac{\partial C_d}{\partial t} = \frac{DC_d}{Dt} - \nabla C_d \mathbf{v}^* \quad (24)$$

By substituting Eq. (24) into the l.h.s. of Eq. (19), the l.h.s. of the governing equation with the linear isotherm becomes

$$\begin{aligned} &(\theta + \rho_0^m K_d) \frac{\partial C_d}{\partial t} + \mathbf{v} \nabla C_d \\ &= (\theta + \rho_0^m K_d) \left( \frac{DC_d}{Dt} - \nabla C_d \mathbf{v}^* \right) + \mathbf{v} \nabla C_d \\ &= \frac{DC_d}{Dt} (\theta + \rho_0^m K_d) + \nabla C_d (\mathbf{v} - \mathbf{v}^* (\theta + \rho_0^m K_d)) \end{aligned} \quad (25)$$

Substituting the seepage velocity, Eq. (23), into Eq. (25), the advective term vanishes

$$(\theta + \rho_0^m K_d) \frac{\partial C_d}{\partial t} + \mathbf{v} \nabla C_d = \frac{DC_d}{Dt} (\theta + \rho_0^m K_d) \quad (26)$$

Back substituting Eq. (26) into Eq. (19) gives the governing equation in a Lagrangian formulation

$$\begin{aligned} &\frac{DC_d}{Dt} (\theta + \rho_0^m K_d) \\ &= \text{div}(\mathbf{D}_m \cdot \nabla C_d) + \left( \tilde{\theta} \frac{\partial h}{\partial t} - \frac{\partial \theta}{\partial t} \right) C_d \end{aligned} \quad (27)$$

This no longer includes the hyperbolic advective term. The mastic transport equation could now be solved using a full implementation of the Lagrangian approach, i.e. using a moving coordinate system. Because of the challenges that may occur due to a highly deforming grid, in this research a mixed Lagrangian-Eulerian approach is

implemented, whereby the advective term of the total material time derivative  $\frac{DC_d}{Dt}$  is separately evaluated in a Lagrangian manner by a single-step reverse particle tracking methodology. In the following the principle of the particle tracking methodology is explained.

### 3.3 Particle tracking methodologies

In the original particle tracking method, suggested by Gardner [Gardner et al., 1964], advection is handled by the method of characteristics applied to a set of moving particles. The diffusion part of the problem is solved by an explicit finite difference scheme on a fixed grid. Although this method is virtually free of numerical dispersion, it becomes unstable when the time step size exceeds a certain limit. In order to avoid the need for an independent set of moving particles, Hinstrup et al. [1977] suggested redefining the particles at discrete time intervals so as to make them coincide with the nodes of a fixed difference grid. The position of each particle at intermediate times is obtained by polynomial interpolation between concentration values at surrounding grid points. In the method suggested by Neuman [1981], the advection term is decoupled in an unambiguous manner. Since the advection and the diffusion problems require different treatments, they are solved on separate space-time grids. The nodes of these grids may coincide at selected points. The spatial grids are fixed, but there is nothing in the method to prevent them from being deformed. The method consists of solving the advection problem on one grid by the method of characteristics and projecting the results back. Because of its numerical advantages and its ability to handle a deforming grid, this method has been applied to the research described in this paper.

### 3.4 Single-step reverse particle tracking methodology

By formulating the total material time derivative of the desorbed concentration and replacing the partial time derivative of the governing equation, Eq. (27) no longer include the advective term.

The material time derivative  $\frac{DC_d}{Dt}$  can be approxi-

mated by

$$\frac{DC_d(\mathbf{x}, t)}{Dt} = \frac{C_d(\mathbf{x}_{t+\Delta t}, t + \Delta t) - C_d^*(\mathbf{x}_i^*, t)}{\Delta t} \quad (28)$$

To find the concentration  $C_d^*$  at time  $t$ , consider a fictitious particle that moves from a location  $\mathbf{x}_i^*$  at time  $t$  to a new location  $\mathbf{x}_i$  at time  $t + \Delta t$ , the latter coinciding with node  $n$ , Figure 3.

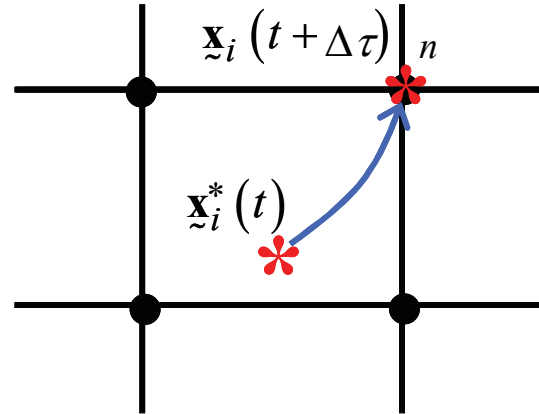


Figure 3: Movement of a fictitious particle

Since the movement of the particle is along the characteristic line with the seepage velocity  $\mathbf{v}^*$ , Eq. (23), the initial particle location  $\mathbf{x}_i^*(t)$  can be found from

$$\mathbf{x}_i^*(t) = \mathbf{x}_i(t + \Delta \tau) - \int_t^{t + \Delta \tau(\mathbf{x}_i^*)} \mathbf{v}^* dt \quad (29)$$

where the time integral is taken along the particle flow path. If  $\mathbf{x}_i^*(t)$  is located outside of the element under consideration  $\Delta \tau(\mathbf{x}_i)$  shall be reduced such that  $\mathbf{x}_i^*(t)$  will be located within the element boundaries.

Once the backward particle position  $\mathbf{x}_i^*(t)$  is known, the corresponding concentration  $C_d^*(\mathbf{x}_i^*, t)$  can be obtained by interpolating between nodal values according to

$$C_d^*(\mathbf{x}_i^*, t) = \sum_{j=1}^n C_j(t) N_j(\mathbf{x}_i^*(t)) \quad (30)$$

The diffusion equation  $\text{div}(\mathbf{D}_m \cdot \nabla C_d)$  is then solved using a fixed (Eulerian) coordinate system.

For a steady-state simulation, where  $\Delta t \rightarrow \infty$ , the logic is implemented by multiplying the transient storage term by zero and evaluating the advection term in a fixed coordinate system.

### 3.5 Weighted residual formulation

The weak form of the governing equation with the linear isotherm, can be found by multiplying Eq. (27) with a weighting function  $w_i$  and integration over the domain

$$\int_V w_i \left[ \frac{DC_d}{Dt} (\theta + \rho_0^m K_d) - \text{div}(\mathbf{D}_m \cdot \nabla C_d) \left( \tilde{\theta} \frac{\partial h}{\partial t} - \frac{\partial \theta}{\partial t} \right) C_d \right] dV = 0 \quad (31)$$

Integrating by parts and making use of the divergence theorem, Eq. (31) yields

$$\begin{aligned} \int_V w_i \frac{DC_d}{Dt} (\theta + \rho_0^m K_d) dV - \int_S \mathbf{n} w_i \mathbf{D}_m \cdot \nabla C_d dS \\ + \int_V (\mathbf{D}_m \cdot \nabla C_d \nabla w_i) dV \\ - \int_V w_i \left( \tilde{\theta} \frac{\partial h}{\partial t} - \frac{\partial \theta}{\partial t} \right) C_d dV = 0 \quad (32) \end{aligned}$$

The variable desorbed concentration term can be approximated by a summation of the nodal values  $j$  multiplied by a shape function  $N_j$

$$C_d = \sum_{j=1}^n N_j C_j^d \quad (33)$$

Since the weighting functions  $w_i$  can be taken equal to the shape functions  $N_i$ , in the Galerkin method

$$w_i = N_i \quad (34)$$

Replacing Eq. (33) and Eq. (34) into Eq. (32) and summing over the volumes of the individual elements, the finite element approximation of the

governing equation becomes

$$\begin{aligned} \sum_{j=1}^n \left( \int_V N_i (\theta + \rho_0^m K_d) N_j dV \right) \frac{DC_j^d}{Dt} \\ + \sum_{j=1}^n \left( \int_V (\nabla N_i \mathbf{D}_m \cdot \nabla N_j) dV \right) C_j^d \\ - \sum_{j=1}^n \left( \int_V N_i \left( \tilde{\theta} \frac{\partial h}{\partial t} - \frac{\partial \theta}{\partial t} \right) N_j dV \right) C_j^d \\ = \int_S \mathbf{n} N_i \mathbf{D}_m \cdot \nabla C_d dS \quad (35) \end{aligned}$$

This equation is solved using a pointwise iterative solver which employs the basic successive iterative method, including the Gauss-Seidel method [Bathe, 1996], [Press et al. 1986].

## 4 Numerical analyses

### 4.1 Numerical oscillation and numerical dispersion

The accurate computational modeling of an advection-diffusion transport equation, especially in the presence of an advection-dominated term, with either a discontinuity or steep gradient of the dependent variable, has been addressed to varying degrees of success in the field of computational fluid dynamics [Ahrem et.al. 2007]; [Arefmanesh et.al 2008]; [Han et.al 2007] [LeV-que 1992], [Morton 1980]; [Quarteroni and Valli 1976], [Ganzha and Vorozhtsov 1998], [Wang and Hutter 2001]; [Atluri 1998, 2006]; [Selvadurai and Dong 2006 (a),(b)]; [XueHong et.al 2007]. Higher-order methods require the size of the domain discretization element to be small enough, such that the elemental Péclet number, Eq.(20), should not be greater than unity.

When the elemental Péclet number is greater than unity the methods give rise to unrealistic numerical phenomena such as oscillations, negative concentrations and artificial diffusion at regions close to a leading edge with a discontinuous front. For this reason, in conventional higher-order methods for advection dominated problems, a finer mesh is invariably used throughout the region,

since the velocity field is usually not known *a priori*. This places a great demand on computational resources, particularly in simulations involving three-dimensional problems. The first order methods such as the Lax-Friedrich scheme, on the other hand, eliminate the oscillatory behavior at discontinuous fronts, where there is no physical diffusion (i.e.  $Pe = \infty$ ), but gives rise to numerical dispersion in the solution. This feature is generally accepted for purpose of the engineering usage of the procedures, but from a computational point of view gives rise to strong reservations concerning the validity of the procedures developed for the advection-diffusion transport equation for the solution of the purely advective transport problem. Furthermore, if physical diffusive phenomena are present in the transport problem, it becomes unclear as to whether the diffusive patterns observed in the solution are due to the physical process or an artifact of the numerical scheme.

Evaluating the accuracy of the purely advective transport problem is therefore a necessary prerequisite to gaining confidence in the application of the computational scheme to the study of the advection-diffusion problem. The real test for a computational scheme developed for modeling the advection dominated transport problem is to establish how accurately the computational scheme can converge to the purely advective transport problem at zero physical diffusion.

#### 4.2 Validation of purely advective transport

The validation of the presented numerical approach is made by comparing the computational results with two one-dimensional exact closed form solutions involving the advective transport problem.

##### Validation 1

For the first validation, a finite element mesh of length  $L_x = 10$  mm with negligible  $y$  and  $z$  dimensions is exposed to a water flow field of constant velocities  $v_x = v_0$  and  $v_y = v_z = 0.0$  mm/s, Figure 2. The region is assumed fully saturated and the diffusion tensor  $\mathbf{D}_m$  is zero. At time  $t = 0.0$  s the region is subjected to a discontinuous desorbed mastic concentration front at the boundary in the form of a Heaviside step function  $H(t)$ .

These conditions reduce the mastic transport equation Eq. (19) to a one dimensional purely advective transport equation of the form

$$\frac{\partial C_d}{\partial t} + v_0 \nabla C_d = 0 \quad (36)$$

With the boundary conditions

$$\begin{aligned} C(0, t) &= C_0 H(t) \\ C(x, 0) &= 0.0 \end{aligned} \quad (37)$$

The exact analytical development of the desorbed mastic concentration field can in this case be found as [Selvadurai, 2008]

$$C_d(\mathbf{x}, t) = C_0 H \left[ t - \frac{x}{v_0} \right] \quad (38)$$

In Figure 3 the numerical solutions for  $v_0 = 1.0$  mm/s and  $C_0 = 1.0$  at  $x = 10.0$  mm are compared to the exact analytical solution for various mesh refinements, whereby using a constant Courant number,  $Cr$ , equal to 1.0

$$Cr = \frac{|v_x| dt}{h_x} \quad (39)$$

where  $dt$  is the time step and  $h_x$  is the element size.

It can be seen from Figure 3 that with increased mesh refinement, the numerical diffusion is reduced and the concentration front is simulated quite accurately without oscillatory effects. It may be observed that none of the discretizations exhibit any numerical oscillation.

Varying  $Cr$ , i.e. the time-step, shows that for a constant discretization of 50 elements, i.e.  $h_x = 0.2$  mm, higher values of  $Cr$  actually lead to a better approximation, Figure 4. This means that the solution seems to improve for an increasing time-step. The reason for this can be found in the fact that for a larger time-step, less time-steps are needed, which reduces the accumulating numerical error. For  $Cr$  values smaller than 1, i.e. a time step of  $dt \leq 0.2$  s the solution converges to a constant solution. Another comment that must be made here is that the particle tracking algorithm automatically reduces the time-step if the particle

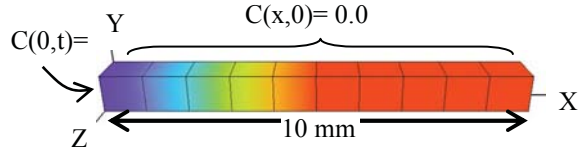


Figure 4: Finite element discretization for 10 elements,  $h_x = 1.0$  mm

is not within the boundaries of the element, Eq. (29).

A finite element mesh with a chosen  $dt$  that is too big to capture the particles will therefore automatically be reduced. In this, the algorithm adjusts the Courant number itself if necessary.

This observation is confirmed by plotting the movement of the concentration front at time  $t = 2$  s for  $Cr$  values equal to 1.0 and 10, Figure 5. The two curves show a distinct difference in numerical dispersion, where the computation with  $Cr = 10$  i.e.  $dt = 2.0$  s, approximates the advective front quite accurately.

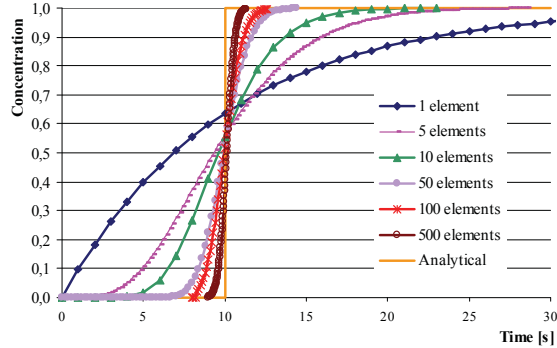


Figure 5: Simulation of the advection front,  $Cr = 1.0$

### Validation 2

For the second validation, the same finite element mesh is exposed to a changing flow field of

$$v_x = v_0 \exp(-\lambda t) \quad (40)$$

and  $v_y = v_z = 0.0$  mm/s, Figure 2. The region is assumed fully saturated with negligible water capacity  $\tilde{\theta}$  and a zero diffusion tensor,  $\mathbf{D}_m$ . At time  $t = 0.0$  s the same boundary conditions as in the first validation are assumed, Eq. (37).

These conditions simplify the mastic transport equation to the form

$$\frac{\partial C_d}{\partial t} + v_0 \exp(-\lambda t) \nabla C_d = 0 \quad (41)$$

and the developing desorbed mastic concentration field under these conditions can be found analytically as [Selvadurai, 2008]

$$C_d(\mathbf{x}, t) = C_0 H \left[ \frac{[1 - \exp(-\lambda t)]}{\lambda} - \frac{x}{v_0} \right] \quad (42)$$

Because the velocity field is time dependent, the Courant number is not constant either and can be found from

$$Cr = \beta \exp(-0.02t) \quad (43)$$

In Figure 6 the numerical solutions at  $x = 10.0$  mm with  $v_0 = 1.0$  mm/s,  $C_0 = 1.0$ ,  $\beta = 1.0$  and  $\lambda = 0.02$  s<sup>-1</sup> are compared to the analytical solution Eq. (42) for various mesh refinements. It can be seen that for the case under consideration an increased refinement of 500 elements, with  $h_x = 0.02$  mm and  $dt = 0.02$  s, approximates the analytical solution with negligible numerical dispersion. Again, none of the discretizations showed any signs of numerical oscillations in the approximation.

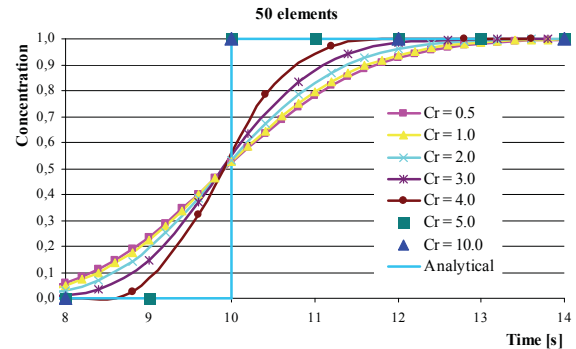


Figure 6: Courant number analysis for the mesh with 50 elements

By comparing the solution of the constant finite element discretization of 50 elements with a  $Cr$  values with  $\beta = 0.5$  and  $\beta = 1.0$ , it can be shown that a higher  $Cr$  value again leads to a more accurate solution, Figure 7.

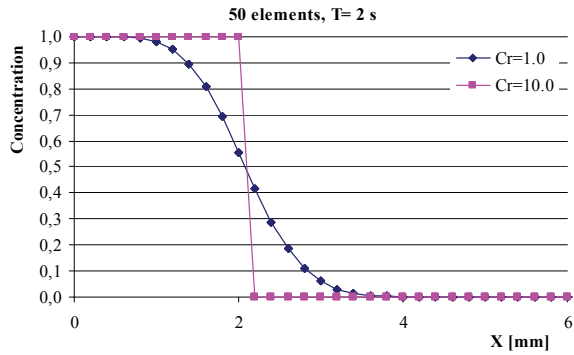


Figure 7: Movement of the concentration front at  $T = 2$  s for  $Cr = 1.0$  and  $Cr = 10$

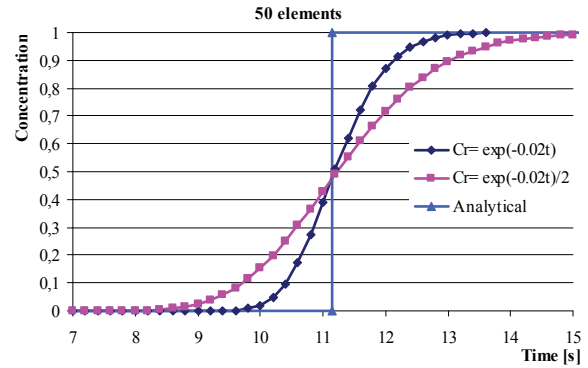


Figure 9: Courant number analysis for the mesh with 50 elements

### 4.3 Advective transport in an asphaltic mix

To demonstrate the change in response of an asphaltic mix, when mastic erosion occurs, a finite element mesh of two aggregates, coated in a mastic film is made, Figure 10. Between the coated aggregates a macro-pore is situated which is assumed fully saturated. The macro-pore is simulated with a porous media element [Liu 2005].

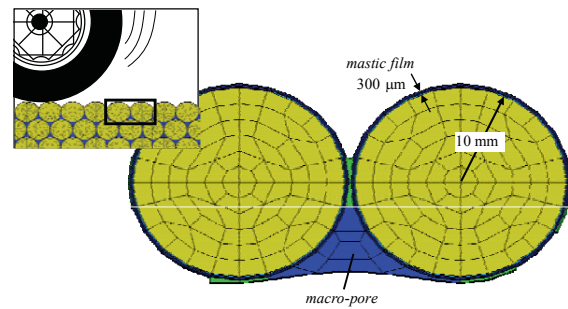


Figure 10: Finite element discretization

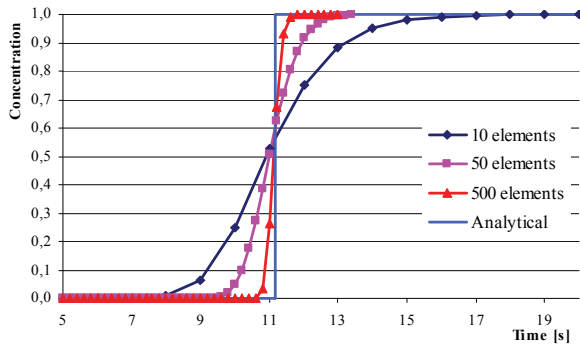


Figure 8: Simulation of the advection front, with  $Cr = \exp(-0.02t)$

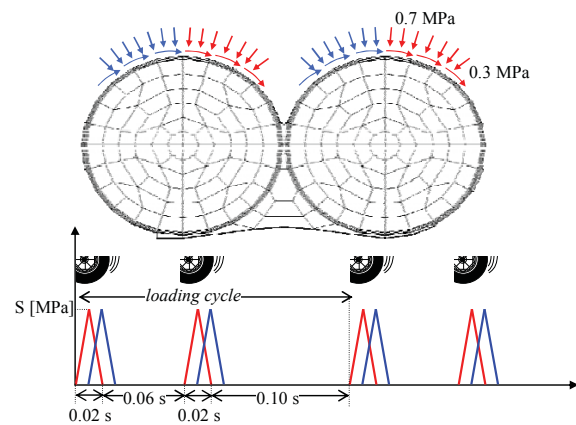


Figure 11: Imposed loading conditions

Since the two aggregates are situated on the top layer of the asphalt wearing surface, they are in direct contact with the traffic loading. This loading condition is simulated with a cyclic loading, with a maximum compressive stress of 0.7 MPa and a maximum shearing stress of 0.3 MPa, Figure 11.

The stones are assumed hyper-elastic and the mastic film is simulated with a elasto-visco-plastic

material model [Scarpas 2000, 2005], [Scarpas et.al 2006], [Kringos 2007]. The aggregates are exposed to numerous loading cycles. Each loading cycle, the saturated macro-pore develops excessive water pressure gradients, which invoke erosion damage at the mastic films which are in direct contact with the water [Kringos

and Scarpas 2005(a), 2005(b)], [Kringos 2007], [Kringos et.al.2007].

Depending on the value chosen for  $K_d$ , see Eq. (18), it can be shown that in addition to mechanical damage due to the loading, additional damage is generated. In Figure 12, the equivalent plastic strain  $\xi$ , which is a measure for damage, is shown for a node which is located in the mastic film for various  $K_d$  values. Figure 13 shows the impact on the resulting stress-strain response.

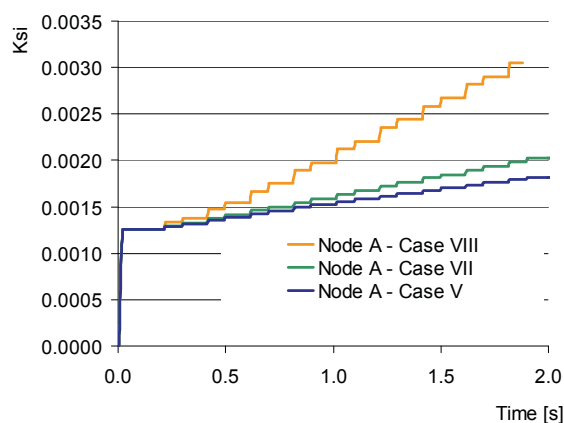


Figure 12: Damage development

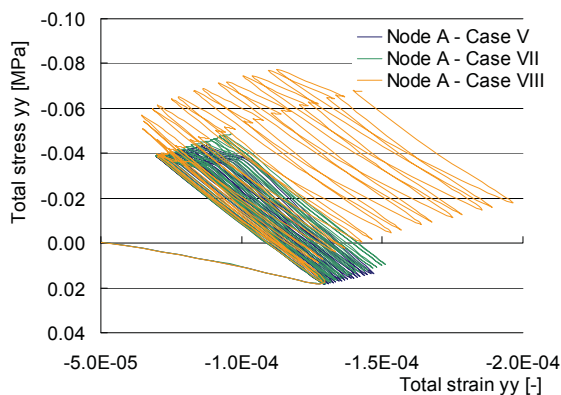


Figure 13: Stress-strain response

## 5 Conclusions

A Hybrid Lagrangian-Eulerian method is used in combination with a single step reverse particle tracking algorithm to develop an oscillation-free and non-diffusive computational solution for the

advective-diffusive transport of mastic particles from an asphaltic mix when exposed to a water flow field. It is shown from the numerical validations that the methodology can give an oscillation-free and non-dispersive solution for the case of a purely advective transport. A finer finite element mesh was shown to give better solutions for constant Courant numbers. When keeping the discretization constant, a higher Courant number seemed to give a better solution. This can be explained by the fact that for a larger time-step, less time-steps are needed, which reduces the accumulating numerical error. For  $Cr$  values smaller than 1, i.e. a time step of  $dt \leq 0.2s$  the solution converges to a constant solution. Because the particle tracking algorithm automatically reduces the time-step if the particle is not within the boundaries of the element, the algorithm adjusts the Courant number itself if necessary.

Even though the numerical validations showed that to capture advection dominated transport a relatively large time-step can be used, it should be kept in mind that in general the diffusion tensor  $\mathbf{D}_m$  of the mastic shall not be zero. Since, for the simulation of mastic diffusion, a smaller time step will increase the accuracy of the approximation, an optimum value for the time-step must be found when simulating transport due to both advection and diffusion.

Having shown that the algorithm implemented in RoAM is able to accurately capture advective transport of mastic particles, the research will continue with evaluating the importance of the contribution of this phenomenon to the overall moisture damage in open-graded asphaltic mixes. Currently experimental studies are being performed toward relating the mix-permeability to loss of mastic due to a fast water flow, which will give a better insight into the desorption curve of the mastic, Eq. (18).

The ultimate goal of this research is not only to improve the insight of the causes and the effects of the different phenomena that cause raveling in asphalt, but moreover to enable the road authorities via determination of fundamental material parameters to make improved asphalt mix design and better long-term road maintenance strategies.

## References

- Ahrem R.; Beckert A.; Wendland H.** (2006): A Meshless Spatial Coupling Scheme for Large-scale Fluid-Structure interaction Problems, *CMES: Computer Modeling in Engineering & Sciences*, Vol.12, 2.
- Arefmanesh A.; Najafi M.; Abdi H.** (2008): Meshless Local Petrov-Galerkin Method with Unity Test Function for Non-Isothermal FLuid FLOW, *CMES: Computer Modeling in Engineering & Sciences*, Vol.25, 1.
- Atluri S.N.; Zhu T.** (1998): A new meshless local Petrov-Galerkin approach in computational mechanics, *Journal of Computational Mechanics*, Vol.22, pp. 117-127.
- Atluri S.N.; Liu H.T.; Han Z.D.** (2006): Meshless Local Petrov-Galerkin Mixed Finite Difference Method for Solid Mechanics, *CMES: Computer Modeling in Engineering & Sciences*, Vol.15, 1, pp. 1-16.
- Baptista A.M.; Adams E.E.; Stolzenback K.D.** (1984): The 2-D Unsteady Transport Equation Solved by the Combined use of the Finite Element Method and the Method of Characteristics, in *Proceedings of the 5<sup>th</sup> Int. Conf. on FE in Water Resources*, Springer-Verlag, pp. 353-362.
- Bathe K.-J.** (1996): *Finite Element Procedures*, Prentice Hall, pp. 747.
- Belytschko T.; Liu W.K.; Moran B.** (2000): *Nonlinear Finite Elements for Continua and Structures*, John Wiley & Sons Ltd.
- Casulli, V.** (1987): Eulerian-Lagrangian Methods for Hyperbolic and Convection Dominated Parabolic Problems, in: *Computational Methods for Nonlinear Problems*, edited by R.L. Taylor, D.R.J. Owen and E. Hinton, pp. 239-269.
- Douglas J.; Russel T.F.** (1982): Numerical Methods for Convection Dominated Diffusion Problems Based on Combining the Method of Characteristics with Finite Element or Finite Difference Procedures, *SIAM J. Numerical Analyses*, Vol.19, pp. 871-885.
- Galeati G.; Gambolati G.; Neuman S.P.** (1992): Coupled and Partially Coupled Eulerian-Lagrangian Model of Freshwater-Seawater Mixing, *Water Resources Research*, 28.
- Gardner A.O.; Peaceman D.W.; Pozzi A.L.** (1964): *Society of Petroleum Engineering Journal*, Vol. 4, 26-36.
- Ganzha V.G.; Vorozhtsov E.V.** (1998): *Computer aided analysis of different schemes for partial differential equations*, CRC Press, Boca Raton.
- Han K.; Feng T.; Owen, D.R.J.** (2007): Numerical Simulation of Irregular Particle Transport in Turbulent Flows Using Coupled LBM-DEM, *CMES: Computer Modeling in Engineering & Sciences*, Vol. 18,2.
- Hindrup P.; Kej A.; Kroszynski U.** (1977): in: *Proceedings XVIII International Association Hydraulic Res. Congress*, Baden-Baden, Germany, Vol.13, pp. 129-137.
- Hughes T.J.R.** (1987): *The Finite Element Method: Linear Static and Dynamic Finite Element Analysis*, Dover Publications Inc.
- Jong, E. de** (1999): *Wegbouwkundige Werkdagen*, the Netherlands.
- Kringos N.; Scarpas A.** (2005(a)): Raveling of Asphaltic Mixes Due to Water Damage: Computational Identification of Controlling Parameters, *Journal of Transportation Research Board*, No. 1929, Bituminous Paving Mixtures, p.79-87
- Kringos N.; Scarpas A.** (2005(b)): *Simulation of Combined Mechanical-Moisture-induced Damage in Asphaltic Mixes*, Edit: Scarpas A. and Kringos N, *International Workshop on Moisture-induced Damage*, Delft, the Netherlands, November 2005, ISBN-13: 978-90-816396-1-1.
- Kringos N.; Scarpas A.; Kasbergen C.** (2007): Three Dimensional Elasto-Visco-Plastic Finite Element Model for Combined Physical-Mechanical Moisture Induced Damage in Asphaltic Mixes, *Journal of the Association of Asphalt Paving Technologists*, Vol. 76.
- Kringos N.** (2007): *Modeling of Combined Physical-Mechanical Moisture Induced Damage in Asphaltic Mixes*, PhD dissertation, TU Delft, ISBN 978-90-9021765-9.
- LeVeque R.J.** (1992): *Numerical method for conservation laws*, Birkhäuser Verlag Basel-Boston

Berlin.

**Liu X.; Scarpas A.; Blaauwendraad J.** (2005): Numerical modelling of nonlinear response of soil. Part 1: Constitutive model, *International Journal of Solids and Structures*, Vol.42, 7, p.1849-1881.

**Neuman S.P.** (1981): A Eulerian-Lagrangian Numerical Scheme for the Dispersion-Convection Equation Using Conjugate Space-Time Grids, *J. of Computational Physics*, Vol.41, pp. 270-294.

**Neuman S.P.** (1984): Adaptive Eulerian-Lagrangian Finite Element Method for Advection-Dispersion, *Int. J. Numerical Methods Eng.*, Vol.20, pp.321-337.

**Morton K.W.** (1980): Stability of finite difference approximations to a diffusion-convection equation, *Int. Journal Numerical Methods in Engineering*, Vol.15, pp.677-683.

**Press W.H.; Flannery B.P.; Teukolsky S.A.; Vetterling W.T.** (1986): *Numerical Recipes*, Cambridge University Press.

**Quarteroni A.; Garder A.** (1976): Selective damping in a Galerkin method for solving wave problems with variable grids, *Monthly Weather Rev.*, Vol.104, pp. 1583-1590.

**Scarpas A.** (2000): CAPA-3D Finite Element System Users Manual I, II and III, a *Delft University of Technology Publication*.

**Scarpas A.** (2005): *A Mechanics based Computational Platform for Pavement Engineering*, ISBN 90-9019040-6.

**Scarpas A.; Kasbergen, C.; Kringos, N.** (2006): Energy based, *Three Dimensional Elasto-Visco-Plastic Constitutive Model for Asphalt Concrete Response*, Research Progress Report, Section of Structural Mechanics, Faculty of Civil Engineering and Geosciences, Delft University of Technology.

**Selvadurai, A.P.S.** (2000): *Partial Differential Equations in Mechanics*, Vol.1. Springer Verlag.

**Selvadurai A.P.S.; Dong W.** (2006(a)): A time adaptive scheme for the solution of the advection equation in the presence of a transient flow velocity, *CMES: Computer Modeling in Engineering & Sciences*, Vol.12, pp. 41-53.

**Selvadurai A.P.S.; Dong W.** (2006(b)): The numerical modelling for advective transport in the presence of fluid pressure transients, *Int. J. for Numerical and Analytical Meth. in Geomechanics*, Vol. 30, pp. 615-634, doi.10.1002/nag494.

**Selvadurai, A.P.S.** (2008): On non-classical analytical solutions for advective transport problems, *Water Resources Research* (Accepted)

**Wang Y. and Hutter K.** (2001): Comparison of numerical methods with respect to convective dominated problems, *Int. Journal of Numerical Methods in Fluids*, Vol. 37, pp. 721-745.

**XueHong W.; ShengPin S.; WenQuan T.** (2007): Meshless Local Petrov-Galerkin Collocation Method for 2D Heat Conduction Problems, *CMES: Computer Modeling in Engineering & Sciences*, Vol. 22,1.

